This is a repository copy of *Passivating Grain Boundaries in Polycrystalline CdTe*.

Passivating Grain Boundaries in Polycrystalline CdTe

Chuan-Jia Tong*[ORCID] and Keith P. McKenna*[ORCID]

Department of Physics, University of York, Heslington, York YO10 5DD, United Kingdom

S *Supporting Information*

ABSTRACT: Using first-principles density functional calculations, we investigate the structure and properties of three different grain boundaries (GBs) in the solar absorber material CdTe. Among the low $\sum$ value symmetric tilt GBs $\sum 3$ (111), $\sum 3$ (112), and $\sum 5$ (310), we confirm that the $\sum 3$ (111) is the most stable one but is relatively benign for carrier transport as it does not introduce any new states into the gap. The $\sum 3$ (112) and $\sum 5$ (310) GBs, however, are detrimental due to gap states induced by Te−Te and Cd−Cd dangling bonds. We systematically investigate the segregation of O, Se, Cl, Na, and Cu to the GBs and associated electronic properties. Our results show that co-doping with Cl and Na is predicted to be a viable approach passivating all gap states induced by dangling bonds in CdTe.
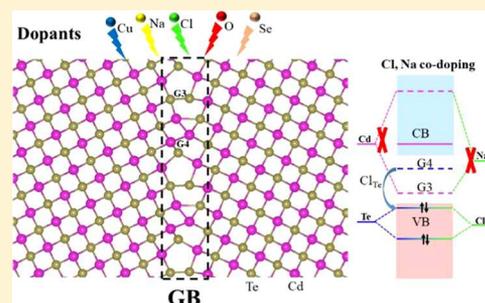
INTRODUCTION

Polycrystalline CdTe has been demonstrated as a leading thin-film solar cell material due to its low cost, ease of manufacturing, and high efficiency.[1−4] As a solar cell absorber, its extraordinary performance mainly comes from a high absorption coefficient and a direct band gap of 1.5 eV, which is ideal for optimal solar conversion.[5] Typically, polycrystalline semiconductor thin films will exhibit poorer photoelectrical properties as compared to their single-crystal counterparts due to the existence of grain boundaries (GBs), which may induce deep gap states and act as nonradiative recombination centers.[6−9] Indeed, as-grown polycrystalline CdTe films exhibit very poor performance due to dangling bonds (DBs) present at GBs. Treatment with CdCl2 significantly improves performance, but it still falls short compared to single crystals. In particular, the open-circuit voltage of the best-treated CdTe films is still more than 120 mV below that of single crystals.[10] Thus, understanding and learning how to passivate detrimental GBs in polycrystalline materials remains a hot topic.

Recently, there have been a series of both experimental and theoretical studies on GBs in CdTe.[11−15] Most of the theoretical studies have only focused on the symmetric tilt $\sum 3$ (111) and $\sum 3$ (112) GB, whose atomic structures have been clearly identified by high-resolution transmission electron microscopy. The presence of Te−Te dangling bonds (DBs) in the $\sum 3$ (112) GB has been shown to produce deep gap states.[16,17] Doping with oxygen or chlorine can effectively passivate these deep defect levels.[18,19] This is consistent with the experimental result that CdCl2 or MgCl2 treatment improves the performance in CdTe solar cells.[20−22] The $\sum 3$ (112) GB that has been studied previously is the Te-core variant that is expected to be the most stable for Te-rich compositions. The alternative Cd-core $\sum 3$ (112) is yet unexplored but may also be present. Furthermore, a much wider variety of GB structures will be present in films. A wide range of dopants is also considered experimentally including

Cu (enhancing p-type doping and reducing the back contact barrier),[23,24] Na (p-type doping and enhancing the grain growth),[25,26] Se (tuning the band gap for efficient carrier separation),[27,28] which have yet to be fully explored theoretically. Therefore, a systematic study of the interaction of these different dopants with GBs and their corresponding electronic properties is very timely.

In this paper, with the help of first-principles calculations, we investigate the structures and properties of three different GBs in CdTe. These are the high-symmetry $\sum 3$ (111) GB, the medium-symmetry $\sum 3$ (112) (both Te-core and Cd-core) GBs, and the low-symmetry $\sum 5$ (310) GB. We find that the $\sum 3$ (111) is the most stable GB with an extremely low formation energy (18 mJ/m²) but is relatively benign as it does not introduce any gap states. Dopants such as O, Se, Cl, Na, and Cu do not have a tendency to segregate to the $\sum 3$ (111) GB. The $\sum 3$ (112) and $\sum 5$ (310) GB, however, behave differently. All of the above dopants except for Se have a strong preference to segregate to the $\sum 3$ (112) GB. The presence of DBs leads to the formation of deep gap states. Importantly, O and Cl dopants can passivate the gap states induced by Te−Te DBs. The situation in $\sum 5$ (310) GB is the most complicated, because it contains both strong Te−Te and Cd−Cd DB. The former induces a gap state close to the conduction band minimum (CBM), while the latter induces a shallow gap state close to the valence band maximum (VBM). Our results show that co-doping with Cl and Na is a viable approach to passivate all gap states.

METHODS

The density functional theory calculations were performed using the projector augmented wave method and implemented

in the Vienna ab initio Simulation Package.[29,30] A cutoff energy of 400 eV for the plane-wave basis set was used throughout all calculations, and the atomic position was fully relaxed until the maximum residual force was less than 0.01 eV/Å. Bulk CdTe was modeled using a cubic unit cell and a $5 \times 5 \times 5$ Monkhorst−Pack[31] k-point sampling scheme. The optimized lattice constant for bulk CdTe was 6.53 Å (close to the experimental value of 6.48 Å) with the Perdew−Burke−Ernzerhof (PBE)[32] functional but yielding an underestimated band gap of 0.78 eV at the same time. Using the more accurate hybrid exchange−correlation functional HSE06[33] with the PBE-optimized structure improved the band gap to 1.55 eV, which is in good agreement with the experiment (∼1.6 eV). A self-consistent lattice optimization using HSE06 ($5 \times 5 \times 5$ k-point mesh) yielding a = 6.49 Å predicts a similar band gap of 1.63 eV. Thus, in the following, we performed HSE06 energy calculations using the PBE-optimized GB configurations to reduce the computational cost.

For the GB calculations, we considered three different GBs in CdTe. These included the high-symmetry $\sum 3$ (111) GB, the $\sum 3$ (112) GB (with both Te-core and Cd-core variants), and the lower-symmetry $\sum 5$ (310) GB. We constructed supercells that contained two GBs separated by at least 28 Å to minimize interactions between the periodically repeated images. The information on the supercells used to model the different GBs is summarized in Table 1. The configurations of

Table 1. Optimized Lattice Constants and Calculated Grain Boundary Formation Energy E_f (using the PBE Functional) of the $\sum 3$ (111), $\sum 3$ (112), and $\sum 5$ (310) GBs

GB	lattice constants (Å)	E_f (J/m^2)
$\sum 3$ (111)	a = 9.23, b = 9.23, c = 60.30	0.02
$\sum 3$ (112)	a = 9.23, b = 11.30, c = 55.95	0.62
$\sum 5$ (310)	a = 10.29, b = 6.51, c = 82.87	0.66

all GBs were carefully optimized with the PBE functional and a reduced k-point mesh of $3 \times 3 \times 1$ for both $\sum 3$ (111) and (112) GBs, $3 \times 5 \times 1$ for the $\sum 5$ (310) GB. The length of the supercell in the GB normal direction was also optimized. For the $\sum 5$ (310) GB, we screened possible rigid body translation parallel to the GB plane in 0.5 Å intervals in both X and Y

directions, using empirical polarizable shell model potentials similar to those previously applied to model MgO.[34] The GB formation energies (E_f) were defined in the following way

$$E_f = \frac{E_{GB} - N \times E_{bulk}}{2A} \tag{1}$$

where E_{GB} is the total energy of the supercell, which contains the GB, E_{bulk} is the energy per formula unit of bulk CdTe, N is the number of CdTe formula units in the GB supercell, and A is the cross-sectional GB area. All of the formation energies presented in the paper have been obtained using bulk CdTe supercells of the same size (number of atoms), orientation and similar dimensions as the grain boundary supercells (note that the length of the supercell in the GB normal direction can, in general, be slightly different, since for the GB, this is optimized) to ensure that energy differences are well defined. To give an accurate prediction of GB/defect energy levels and band edge positions, we also employed a single γ-point energy calculation with the hybrid HSE06 functional on all PBE-optimized structures for comparison. For the dopants (O, Se, Cl, Cu, Na) in GBs, we fully optimized atomic coordinates for different sites, and the segregation energy was defined as the energy difference between a bulk-like site (in the center of the grain) and a GB site. Here, we focus on neutral substitutional defects since we predict these to be in general more stable than interstitial defects in bulk CdTe in both Cd-rich and Te-rich conditions (in agreement with the previous reports[35]). Of course, interstitial defects can become more stable under different doping conditions (p-type or n-type) and so predictions will depend strongly on the order of the various thin-film processing steps. A detailed investigation of these issues is beyond the scope of the present study but is certainly an important area for future work.

■ RESULTS AND DISCUSSION

Figure 1a−d shows the local atomic structures of $\sum 3$ (111), $\sum 3$ (112) Te-core, $\sum 3$ (112) Cd-core, and $\sum 5$ (310) GBs. There are no DBs in the $\sum 3$ (111) GB, as clearly seen in Figure 1a. The structure in GB region is very similar to the bulk although the stacking sequence changes from zinc blende to wurtzite structure. The Te−Cd bond length at the GB is
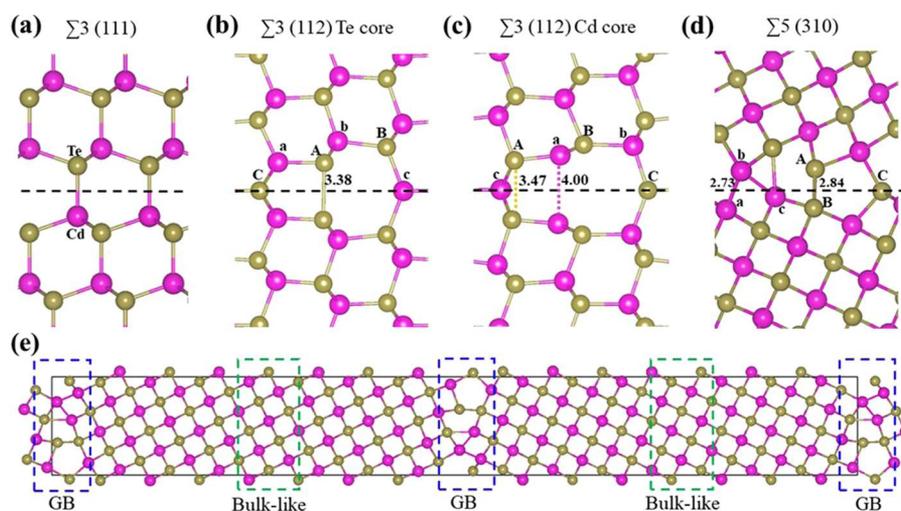
Figure 1. Relaxed atomic structures of (a) $\sum 3$ (111), (b) $\sum 3$ (112) Te-core, (c) $\sum 3$ (112) Cd-core, and (d) $\sum 5$ (310) GBs. Black dashed lines indicate the GB plane. (e) Full supercell used for the $\sum 5$ (310) GB. Brown and pink spheres represent Te atoms and Cd atoms, respectively.
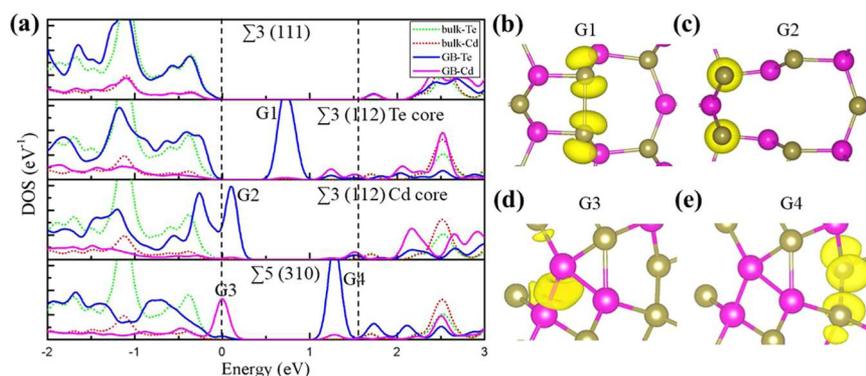
Figure 2. (a) Calculated density of states projected in the bulk-like and GB regions of the $\sum 3$ (111), $\sum 3$ (112) Te-core, $\sum 3$ (112) Cd-core, and $\sum 5$ (310) GBs (from top to bottom). The zero energy is set at the VBM of bulk CdTe. Vertical dashed lines represent the VBM and CBM of bulk CdTe. Calculated charge density associated with the gap states (b) G1, (c) G2, (d) G3, (e) G4, as shown in (a). All results are calculated with HSE06 functional.
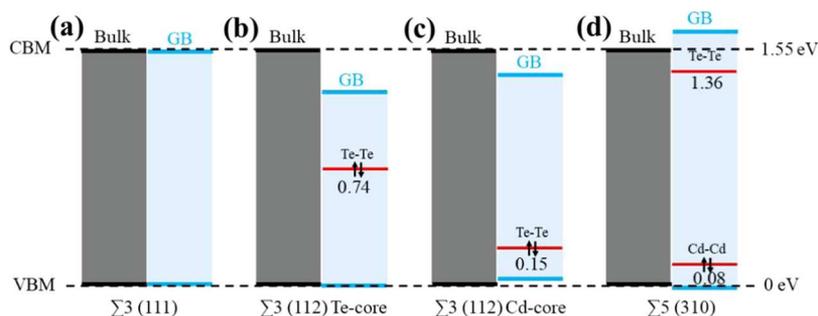
Figure 3. Calculated band edges and defect level positions of different GBs with HSE06 functional. The VBM of pure bulk CdTe is set as zero.

2.82 Å, varying no more than 0.01 Å when compared with the typical bond length in the bulk. Such a high-symmetry configuration results in a tiny grain boundary formation energy of 0.018 J/m^2 (as shown in Table 1), which indicates that the $\sum 3$ (111) GB should be the most stable one in CdTe. The $\sum 3$ (112) GB is another stable GB seen experimentally, and the calculated formation energy is 0.62 J/m^2, which is also quite small. As shown in Figure 1b, the Te-core $\sum 3$ (112) GB has two undercoordinated Te atoms (site A), forming a DB whose length is 3.38 Å, about 1.23 Å shorter than the shortest Te−Te distance in bulk CdTe (4.61 Å). Previous reports[16,18] have confirmed that it is this Te−Te DB that induces a deep gap state that is detrimental. The situation is very similar in the Cd-core $\sum 3$ (112) GB (Figure 1c); however, here the Cd atom (site A) is undercoordinated instead of Te. But the interaction between these two undercoordinated Cd atoms is weaker due to a longer separation (4.00 Å). This GB also contains a Te−Te bond (site A) with a length of 3.47 Å although both Te atoms are fully coordinated to Cd. This weak interaction has a strong influence on electronic properties (see details in Figure 2a). The last GB is the low-symmetry $\sum 5$ (310), as shown in Figure 1d. The calculated formation energy of this GB is 0.66 J/m^2, very close to that in $\sum 3$ (112), which indicates that it could also be expected to be present on thermodynamic grounds. More generally, high-site-coincidence low-sigma grain boundaries such as these are seen experimentally in a wide range of materials[36−39] and there is no reason why CdTe should be an exception. We note that, for example, the $\sum 9$ GB in CdTe has been observed experimentally.[13,40] This configuration is the most complicated because it contains both Te−Te and Cd−Cd DBs. These DBs are much stronger with bond lengths of 2.84 Å for Te−Te and 2.78 Å for Cd−

Cd. Therefore, it will be of great significance to know how these stronger DBs affect the properties of this GB. Figure 1e shows the full supercell for the $\sum 5$ (310) GB. As described in the Methods section, there are two identical GB regions (dashed blue boxes) in our computational model and two bulk-like regions in the center of the grain (20 Å away from GB), as shown in green boxes. Similar supercells are employed for the other GBs, and all structures are provided in the Supporting Information.

To characterize the electronic structure of these GBs, we calculate the density of states (DOS) projected onto atoms in the vicinity of the GB and the bulk-like region (calculated at the HSE level), as shown in Figure 2a. The energy zero is aligned with respect to the VBM of pristine bulk CdTe unit cell. For the $\sum 3$ (111) GB, it is clearly seen that the partial DOS (PDOS) for the GB region almost fully overlaps with that for the bulk. This is because GB has a very similar structure as the bulk. There is no gap state here which confirms it is a benign GB. For the Te-core $\sum 3$ (112), there is a deep gap state (G1) inside the band gap, as reported in previous works. Figure 2b shows the charge density corresponding to this fully occupied deep gap state. It reveals that the charge is highly localized around the Te DB atoms, which once again illustrates that the Te−Te DB is responsible for the deep gap state in the Te-core $\sum 3$ (112) GB. Further analysis indicates that the Te−Te antibonding interaction pushes the state created by the DB away from the VBM and makes it a deeper level. The deep localized gap state is an effective nonradiative recombination center and, therefore, detrimental to solar cell performance.

For the $\sum 3$ (112) Cd-core GB, although there is no deep state inside the band gap, a shallow gap state (G2) still appears close to the VBM. Normally, a shallow state may not accelerate

the recombination too much compared with a deep one, but it still plays a vital role in other aspects such as reducing the open-circuit voltage, inducing the charge transfer, and so on. The charge density in Figure 2c reveals that G2 is associated with the Te−Te bond mentioned above. Combined with the results in the Te-core $\sum$3 (112), we can conclude that the gap state is also related to a Te−Te antibonding state (note that the valance band has primarily Te character, as shown in Figure 2a). We note that a similar result was recently shown for the case of the Te antisite defect in CdTe.[41] The shorter Te−Te bond for the Te-core leads to a stronger interaction between the Te atoms and, therefore, a higher energy of the gap state. For the most complicated $\sum$5 (310) GB, the PDOS clearly shows that there are two shallow gap states. One is close to the VBM (G3), and the other is close to the CBM (G4). From the localized charge distribution in Figure 2d−e, we can see that it is the Cd−Cd and Te−Te DBs that are responsible for gap states G3 and G4, respectively. Moreover, as the Te−Te interaction is the strongest in this GB, the corresponding gap state (G4) has the highest energy of all of the GBs. We obtain qualitatively similar results using the PBE functional (where we are able to use denser k-point grids) except for the reduced bulk gaps and different absolute positions of the gap states.

Figure 3 shows a simplified energy level diagram indicating the position of band edges in the bulk and the GBs as well as the positions of the various gaps. The deep gap state originating from Te−Te DB in the $\sum$3 (112) Te-core GB sits in the middle of the band gap (0.74 eV above the VBM of bulk CdTe, as shown in Figure 3b) with two occupied electrons (in the stoichiometric undoped system). As the Te−Te interaction in $\sum$3 (112) Cd-core is weaker than that in Te-core, the corresponding occupied gap state is lowered to 0.15 eV above the VBM (Figure 3c). The situation is reversed in the $\sum$5 (310) GB (Figure 3d) because its Te−Te antibonding interaction is the strongest. So, the gap state moves up to 0.19 eV below the CBM of bulk CdTe but is unoccupied. Meanwhile, a fully occupied shallow gap state associated with Cd−Cd DB appears about 0.08 eV above the VBM. Once again, the band edge positions of $\sum$3 (111) GB are almost exactly the same as those in the bulk (Figure 3a).

The above results show that DBs in CdTe GBs create gap states, which are harmful to performance. We now systematically consider the effects of Cl-, O-, Se-, Na-, and Cu-dopants since they are widely explored in experiments. But first of all, we need to know whether these dopants have a tendency to segregate to GB regions. The segregation energies of all dopants in all GBs are carefully calculated using the HSE06 functional and summarized in Figure 4. They exhibit a very similar trend with results obtained using PBE (Table S1 and Figure S2). A more negative segregation energy indicates a stronger segregation behavior. For the $\sum$3 (112) and $\sum$5 (310) GBs, we have considered three different Te and Cd sites to be substituted in the GB region, marked by capital and lower-case letters in Figure 1b−d. But only one GB site has been considered for both anion and cation substitutions in $\sum$3 (111) due to the equivalence of all Te and Cd atoms. From the results, we can see that the segregation energy of all dopants in $\sum$3 (111) is close to zero (black bars in Figure 4), which means that no segregation behavior occurs in this GB. This agrees well with a previous report,[35] due to the similar structure in GB and bulk-like regions. Similarly, the absolute value of segregation energy for Se_{Te} in all GBs is also relatively
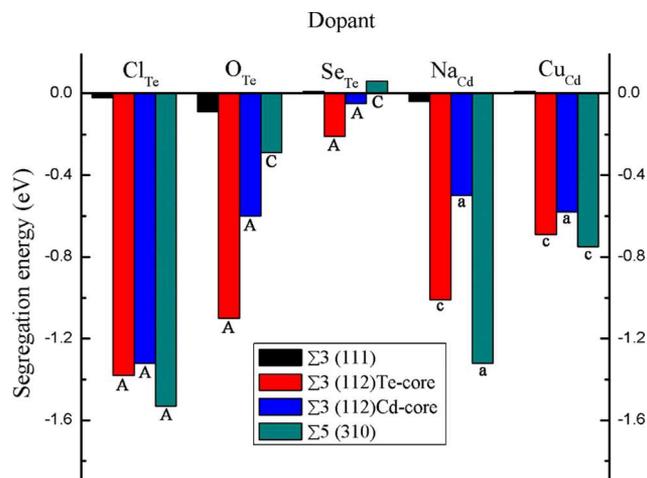
Figure 4. Segregation energy of different dopants in different GBs. The letters under each bar represent the most energetically favorable site in each case. All results are calculated with HSE06 functional.

small, no more than 0.2 eV. As a result, the substituted Se does not show any strong segregation in all GBs, because it is so similar to Te chemically. Also, for this reason, Se segregation does not passivate the DBs and the associated gap states remain.

O and Cl show strong segregation to the $\sum$3 (112) GBs. In both cases, they prefer substituting one of the Te atoms in the DB, namely, site A in Figure 1b,c. But the situation is a little different in the $\sum$5 (310) GB. Cl still favors breaking down the stronger Te−Te DB by segregating to site A (Figure 1d) with the strongest segregation energy (−1.53 eV). This is because Cl has a much smaller atomic size and stronger electronegativity so that it can repel the remaining Te away and increase the Cl−Te distance to 3.40 Å, as shown in the following optimized structure. But the O dopant prefers site C in this GB, probably because the repulsive interaction of O−Te is not strong enough to break down the stronger Te−Te DB, which is confirmed by our following analysis. As for the cation dopants Na and Cu, the segregation energies indicate that they both favor segregating to the GB region. In particular, Na shows a strong tendency to break down the Cd−Cd DB in the $\sum$5 (310) GB with a large segregation energy of −1.32 eV.

The above analysis suggests that all dopants except for Se have a strong preference to segregate to the GBs presenting harmful defect states. Therefore, it is natural to ask whether any of these doped GBs can remove the gap states and improve performance. We have calculated the electronic properties of all energetically favorable doped structures (marked with letters in Figure 4) in $\sum$3 (112) and $\sum$5 (310) GBs. All results are summarized in Figure 5 (a schematic picture showing bonding and antibonding orbital information in $\sum$3 (112) GBs) and Figure 6 ($\sum$5 (310) GB). In fact, Feng et al. have already found that oxygen doping may exhibit a beneficial effect for the Te-core $\sum$3 (112) GB by turning GB-induced deep gap states into less harmful shallow levels inside the valence band.[19] Our results not only confirm their conclusion but also demonstrate that the O substitution in Cd-core $\sum$3 (112) can put the shallow gap state deep G2 inside valence band as well, as shown in Figure 5b. This is because O has a smaller atomic size and stronger electronegativity compared with Te, which increases the O−Te distance so that weakening the O−Te interaction in both Te-core and Cd-core $\sum$3 (112)
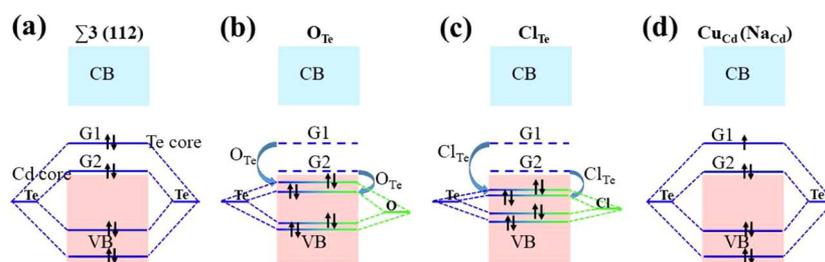
Figure 5. Schematic picture showing how dopants affect gap states in $\sum 3$ (112) GB. G1 and G2 are gap states derived from Te-core and Cd-core, respectively, as shown in Figure 2. Short solid lines represent energy levels of outmost electrons in each element, namely, Te-5p, O-2p, Cl-3p. The small arrows represent electrons occupying each state.
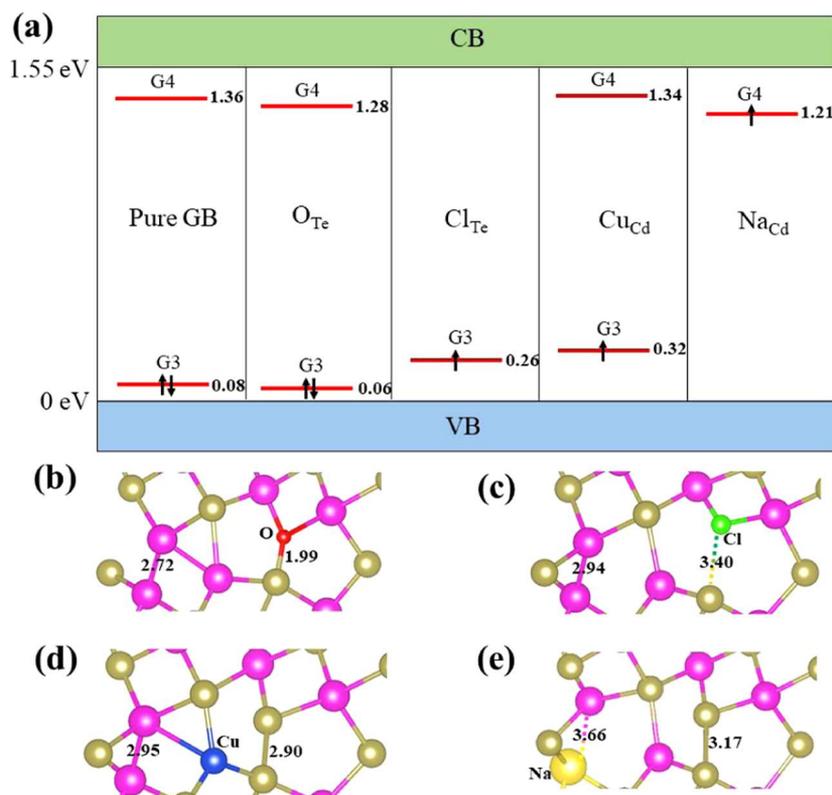
Figure 6. (a) Calculated defect level positions in the pure $\sum 5$ (310) GB and with O_{Te}, Cl_{Te}, Cu_{Cd}, Na_{Cd} dopants using HSE06 functional. The optimized structures of (b) O_{Te}-, (c) Cl_{Te}-, (d) Cu_{Cd}-, (e) Na_{Cd}-doped $\sum 5$ (310) GB. The VBM of pure bulk CdTe is set as zero. Arrows stand for occupied electrons in each state.

GB. Then, antibonding gap states G1 and G2 both move down, clearly shown in Figure 5b. Moreover, Cl-doping has the same function as O-doping and pushes those antibonding levels (G1 and G2) much deeper into the valence band due to much weaker Cl−Te interaction (Figure 5c). With the removal of these harmful gap states, the $\sum 3$ (112) GBs seem to be effectively passivated by anion doping. When it comes to the cation dopants (Na_{Cd}, Cu_{Cd}) in the $\sum 3$ (112) GB, the Te−Te DB length remains almost unchanged and so all gap states still remain close to previous levels (see Figure 5d). Since Na and Cu are p-type dopants, a hole is introduced and the previously fully occupied G1 state becomes half-occupied. This once again demonstrates that the harmful GBs could only be passivated when DBs have been broken down.

In Figure 6, we show the situation for dopants in the $\sum 5$ (310) GB. For O-doping, we choose the case that O substitutes one of the Te atoms in the DB (site A) instead of the more favorable site C, since it is the former that is

associated with the gap state (but we note that both are favorable relative to the bulk). Although O substitution at the DB effectively removes the gap state in the $\sum 3$ (112) GBs, it is not effective for the $\sum 5$ (310) GB, as shown in Figure 6a. This different behavior originates from the different lengths of the Te−Te DB in the GBs. The DB is the shortest (2.84 Å) in the $\sum 5$ (310) GB (Figure 1d) and much longer (3.38/3.47 Å) in the $\sum 3$ (112) GBs (Figure 1b,c). Accordingly, the Te−Te interaction is the strongest in the $\sum 5$ (310) GB and the O dopant atom cannot push away the other Te atom. Instead, Figure 6b shows that the relaxed O−Te bond length decreases to 1.99 Å, far shorter than that in doped $\sum 3$ (112) Te-core (3.42 Å). Consequently, the strong O−Te interaction also induces a deep gap state close to G4 in the pure GB (0.08 eV lower), as shown in Figure 6a. The G3 gap state almost remains unchanged, as the associated Cd−Cd DB length does not change significantly.

The situation for Cl-doping in the $\sum 5$ (310) GB is very different. The fully optimized Cl-doped configuration indicates that the Te–Te DB has been broken (Figure 6c). The longer Cl–Te distance (3.40 Å) weakens the DB interaction, then the antibonding state G4 moves down into the valence band and becomes occupied according to the explanation in Figure 5b. Cl has one more electron than Te, and, as a result, the bonding state G3 becomes half-occupied. Moreover, it has a 0.18 eV upward shift due to the extension of the Cd–Cd DB length when compared with pristine GB. The dopants Cu and Na show different behaviors. Cu prefers segregating to site c, leaving the Te–Te and Cd–Cd DBs (and associated gap states) intact, as shown in Figure 6d. G3 and G4 also remain, except a slight shift of G3 originating from a small variation of Cd–Cd DB length. Once again, the fully occupied G3 becomes half-occupied due to the presence of p-type Cu. Na has a strong tendency to segregate to the GB and break the Cd–Cd DB. Figure 6e clearly shows that G3 has been removed due to the substitution of Na. In the meantime, the Na substitution induces the extension of neighboring Te–Te DB (3.17 Å), which pushes the antibonding state G4 downward (0.34 eV below the CBM of bulk CdTe, as shown in Figure 6a). The original two electrons in G3 together with the hole introduced by Na leave one remaining electron in the gap state G4.

To further test our hypothesis that DB length is a key factor determining the position of gap states at the GBs, we have artificially shortened the O–Te distance in the O-doped $\sum 3$ (112) Te-core from the original length 3.42–1.99 Å, in the direction perpendicular to the boundary plane. The calculated PDOS of structures with different O–Te distances are shown in Figure S3. It shows that a gap state is shifted upward when the O–Te distance is shortened. When the O–Te distance is shortened to 1.99 Å (as found in the O-doped $\sum 5$ (310) GB), a deep gap state close to that in the pure Te-core $\sum 3$ (112) appears in the middle of the gap again. This demonstrates that a deep gap state should be expected if the O–Te DB is short. For Cl, the Cl–Te DB is much longer because their repulsive interaction is stronger due to the fact that Cl has a much smaller atomic size and stronger electronegativity.

From the results above, we can conclude that all gap states can be passivated only when corresponding DBs have been broken. The O dopant can only destroy a weak Te–Te DB such as those in the $\sum 3$ (112) GB but not a stronger one in the $\sum 5$ (310) GB. Cl, on the other hand, is able to remove all Te–Te DBs considered. Na is also effective at breaking Cd–Cd DBs. Therefore, it is natural for us to ask whether Cl–Na co-doping can remove all gap states to effectively passivate this GB? We carry out a further simulation on Cl–Na co-doped $\sum 5$ (310), and the results confirm our hypothesis. For co-doping, we consider two different situations (doping Cl first and doping Na first). We find that the presence of an already segregated Cl dopant increases the segregating energy of a subsequently added Na (from −1.32 to −1.75 eV). On the other hand, the presence of an already segregated Na dopant increases the segregating energy of a subsequently added Cl (from −1.53 to −1.99 eV). GB segregation is favorable for doping in either order but these results suggest that Na followed by Cl should be most favorable. We have also considered the possible formation of a NaCl secondary phase when co-doping with Cl and Na. We found that the NaCl secondary phase is 0.16 eV more energetically favorable than Cl–Na co-doping for the $\sum 5$ (120) grain boundary (these are

total energy differences, excluding entropy contributions, calculated using the HSE06 functional). This small energy difference suggests that the precipitation of NaCl at grain boundaries could take place providing there is a sufficient free space at the grain boundaries. However, this is likely to be a kinetically limited process and so grain boundary doping with Na and Cl should be achievable when given the right processing conditions. Figure 7a shows the fully relaxed
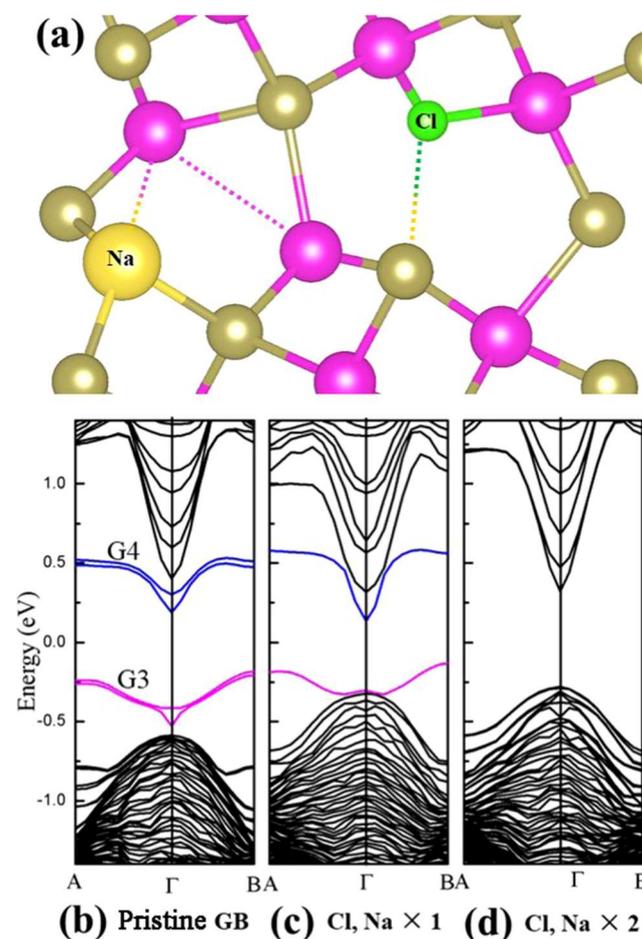
Figure 7. (a) Optimized local atomic structure of Cl–Na co-doped $\sum 5$ (310) GB. Calculated band structures of (b) the pristine, (c) Cl–Na co-doped, and (d) 2 × Cl–Na co-doped $\sum 5$ (310) GB using the PBE functional.

atomic structure of Cl–Na co-doped $\sum 5$ (310) GB. In this case, all DBs have been broken and there are no gap states inside the band gap. We also calculate the band structure around the γ point (Figure 7b), which shows that these gap states (G3 and G4) are in the pure $\sum 5$ (310) GB that are removed following Cl–Na co-doping. Two pairs of Cl–Na dopants are required to eliminate all gap states, as there are two identical GB regions in our supercell. When one of the GB region has been co-passivated by one pair of Cl and Na, half of those gap states disappears inside the band gap, as shown in Figure 7c. Finally, a clean band structure without any gap state appears with the Cl–Na co-doping of both GB regions (Figure 7d).

CONCLUSIONS

In summary, using first-principle calculations, we have systematically investigated three different GBs with five different doped elements. Our calculations employing the hybrid HSE06 functional show that the high-symmetry $\sum 3$ (111) GB is highly stable but relatively benign as it introduces no deep gap states, confirming previous predictions using local or semilocal approximations to exchange and correlation. In addition, none of the dopants studied shows a significant tendency for segregation to this GB due to the similarity between GB and bulk regions. For the other GBs we have considered, we find the following new results: (1) All Te−Te DBs in $\sum 3$ (112) Te-core/Cd-core and $\sum 5$ (310) GBs introduce detrimental gap states. The Te−Te antibonding interaction in $\sum 5$ (310) GB is the strongest due to the shorter bond length, resulting in the highest gap state energy level. The Cd−Cd DB in $\sum 5$ (310) GB introduces a shallow gap state close to the VBM; (2) Se is not helpful for passivating GBs because it shows only a small tendency for GB segregation and does not break down the Te−Te dangling bond leaving the detrimental gap state intact; (3) O can only break weak Te−Te DBs in $\sum 3$ (112) Te-core/Cd-core GBs, while Cl can break all Te−Te DBs. This helps explain why the CdCl$_2$ treatment is so effective. The fact that the Cl does not passivate Cd−Cd dangling bonds, however, is an important point that has previously not been appreciated; (4) Cl−Na co-doping can effectively passivate the $\sum 5$ (310) GB by removing all associated gap states. These results provide atomistic insight into the origins of reduced open-circuit voltage and recombination in polycrystalline CdTe solar cells and suggest practical routes to improve the material performance via doping.

ASSOCIATED CONTENT

ⓈSupporting Information

The Supporting Information is available free of charge on the ACS Publications website at DOI: 10.1021/acs.jpcc.9b08373.

> Full relaxed configurations of $\sum 3$ (111) and $\sum 3$ (112) GBs; segregation energies of all defects at different sites (PDF)

AUTHOR INFORMATION

Corresponding Authors
*E-mail: chuanjia.tong@york.ac.uk (C-.J.T.).
*E-mail: keith.mckenna@york.ac.uk (K.P.M.).

ORCID ◉
Chuan-Jia Tong: 0000-0001-6554-5827
Keith P. McKenna: 0000-0003-0975-3626

Notes
The authors declare no competing financial interest.

ACKNOWLEDGMENTS

REFERENCES

(1) Birkmire, R. W.; McCandless, B. E. CdTe thin film technology: Leading thin film PV into the future. *Curr. Opin. Solid State Mater. Sci.* **2010**, *14*, 139−142.

(2) Kumar, S. G.; Rao, K. S. R. K. Physics and chemistry of CdTe/CdS thin film heterojunction photovoltaic devices: fundamental and critical aspects. *Energy Environ. Sci.* **2014**, *7*, 45−102.

(3) Wang, S.; Wang, L.-W. Exciton Dissociation in CdSe/CdTe Heterostructure Nanorods. *J. Phys. Chem. Lett.* **2011**, *2*, 1−6.

(4) Su, J.; Minegishi, T.; Kageshima, Y.; Kobayashi, H.; Hisatomi, T.; Higashi, T.; Katayama, M.; Domen, K. CdTe-Based Photoanode for Oxygen Evolution from Water under Simulated Sunlight. *J. Phys. Chem. Lett.* **2017**, *8*, 5712−5717.

(5) Okamoto, T.; Yamada, A.; Konagai, M. Optical and electrical characterizations of highly efficient CdTe thin film solar cells. *Thin Solid Films* **2001**, *387*, 6−10.

(6) Metzger, W. K.; Gloeckler, M. The impact of charged grain boundaries on thin-film solar cells and characterization. *J. Appl. Phys.* **2005**, *98*, No. 063701.

(7) McKenna, K. P. Electronic Properties of {111} Twin Boundaries in a Mixed-Ion Lead Halide Perovskite Solar Absorber. *ACS Energy Lett.* **2018**, *3*, 2663−2668.

(8) Wang, Y.; Fang, W.-H.; Long, R.; Prezhdo, O. V. Symmetry Breaking at MAPbI$_3$ Perovskite Grain Boundaries Suppresses Charge Recombination: Time-Domain ab Initio Analysis. *J. Phys. Chem. Lett.* **2019**, *10*, 1617−1623.

(9) Long, R.; Liu, J.; Prezhdo, O. V. Unravelling the Effects of Grain Boundary and Chemical Doping on Electron−Hole Recombination in CH$_3$NH$_3$PbI$_3$ Perovskite by Time-Domain Atomistic Simulation. *J. Am. Chem. Soc.* **2016**, *138*, 3884−3890.

(10) Burst, J. M.; et al. CdTe solar cells with open-circuit voltage breaking the 1 V barrier. *Nat. Energy* **2016**, *1*, No. 16015.

(11) Yan, Y.; Al-Jassim, M. M.; Jones, K. M. Structure and effects of double-positioning twin boundaries in CdTe. *J. Appl. Phys.* **2003**, *94*, 2976−2979.

(12) Sun, C.; Lu, N.; Wang, J.; Lee, J.; Peng, X.; Klie, R. F.; Kim, M. J. Creating a single twin boundary between two CdTe (111) wafers with controlled rotation angle by wafer bonding. *Appl. Phys. Lett.* **2013**, *103*, No. 252104.

(13) Li, C.; et al. Grain-Boundary-Enhanced Carrier Collection in CdTe Solar Cells. *Phys. Rev. Lett.* **2014**, *112*, No. 156103.

(14) Oliveira, J. M.; Malachias, A.; Ospina, C. A.; Ferreira, S. O. Nondestructive Monitoring of Defect Evolution in Epitaxial CdTe Thin Layers Grown on Si(111). *J. Phys. Chem. C* **2014**, *118*, 1968−1973.

(15) Stechmann, G.; Zaefferer, S.; Raabe, D. Molecular statics simulation of CdTe grain boundary structures and energetics using a bond-order potential. *Modell. Simul. Mater. Sci. Eng.* **2018**, *26*, No. 045009.

(16) Park, J.-S.; Kang, J.; Yang, J.-H.; Metzger, W.; Wei, S.-H. Stability and electronic structure of the low-$\sum$ grain boundaries in CdTe: a density functional study. *New J. Phys.* **2015**, *17*, No. 013027.

(17) Liu, C.-Y.; Zhang, Y.-Y.; Hou, Y.-S.; Chen, S.-Y.; Xiang, H.-J.; Gong, X.-G. Self-passivation rule and structure of CdTe $\sum 3$ (112) grain boundaries. *Phys. Rev. B* **2016**, *93*, No. 205426.

(18) Zhang, L.; Da Silva, J. L. F.; Li, J.; Yan, Y.; Gessert, T. A.; Wei, S.-H. Effect of Copassivation of Cl and Cu on CdTe Grain Boundaries. *Phys. Rev. Lett.* **2008**, *101*, No. 155501.

(19) Feng, C.; Yin, W.-J.; Nie, J.; Zu, X.; Huda, M. N.; Wei, S.-H.; Al-Jassim, M. M.; Yan, Y. Possible effects of oxygen in Te-rich $\sum 3$ (112) grain boundaries in CdTe. *Solid State Commun.* **2012**, *152*, 1744−1747.

(20) Major, J. D. Grain boundaries in CdTe thin film solar cells: a review. *Semicond. Sci. Technol.* **2016**, *31*, No. 093001.

(21) Menossi, D.; Artegiani, E.; Salavei, A.; Di Mare, S.; Romeo, A. Study of MgCl$_2$ activation treatment on the defects of CdTe solar cells by capacitance-voltage, drive level capacitance profiling and admittance spectroscopy techniques. *Thin Solid Films* **2017**, *633*, 97−100.

(22) Tuteja, M.; Mei, A. B.; Palekis, V.; Hall, A.; MacLaren, S.; Ferekides, C. S.; Rockett, A. A. $CdCl_2$ Treatment-Induced Enhanced Conductivity in CdTe Solar Cells Observed Using Conductive Atomic Force Microscopy. *J. Phys. Chem. Lett.* **2016**, *7*, 4962−4967.

(23) Perrenoud, J.; Kranz, L.; Gretener, C.; Pianezzi, F.; Nishiwaki, S.; Buecheler, S.; Tiwari, A. N. A comprehensive picture of Cu doping in CdTe solar cells. *J. Appl. Phys.* **2013**, *114*, No. 174505.

(24) Rose, D. H.; Hasoon, F. S.; Dhere, R. G.; Albin, D. S.; Ribelin, R. M.; Li, X. S.; Mahathongdy, Y.; Gessert, T. A.; Sheldon, P. Fabrication procedures and process sensitivities for CdS/CdTe solar cells. *Prog. Photovolt.: Res. Appl.* **1999**, *7*, 331−340.

(25) Sites, J.; Pan, J. Strategies to increase CdTe solar-cell voltage. *Thin Solid Films* **2007**, *515*, 6099−6102.

(26) Kranz, L.; Perrenoud, J.; Pianezzi, F.; Gretener, C.; Rossbach, P.; Buecheler, S.; Tiwari, A. N. Effect of sodium on recrystallization and photovoltaic properties of CdTe solar cells. *Sol. Energy Mater. Sol. Cells* **2012**, *105*, 213−219.

(27) Belyaev, A. P.; Kalinkin, I. P. Conduction processes in inhomogeneous $CdSe_xTe_{1−x}$ semiconductors. *Thin Solid Films* **1988**, *158*, 25−36.

(28) Poplawsky, J. D.; Guo, W.; Paudel, N.; Ng, A.; More, K.; Leonard, D.; Yan, Y. Structural and compositional dependence of the $CdTexSe_{1−x}$ alloy layer photoactivity in CdTe-based solar cells. *Nat. Commun.* **2016**, *7*, No. 12537.

(29) Blöchl, P. E. Projector augmented-wave method. *Phys. Rev. B* **1994**, *50*, No. 17953.

(30) Kresse, G.; Joubert, D. From ultrasoft pseudopotentials to the projector augmented-wave method. *Phys. Rev. B* **1999**, *59*, No. 1758.

(31) Monkhorst, H. J.; Pack, J. D. Special points for Brillonin-zone integrations. *Phys. Rev. B* **1976**, *13*, No. 5188.

(32) Perdew, J. P.; Burke, K.; Ernzerhof, M. Generalized Gradient Approximation Made Simple. *Phys. Rev. Lett.* **1996**, *77*, No. 3865.

(33) Heyd, J.; Scuseria, G. E.; Ernzerhof, M. "Hybrid functionals based on a screened Coulomb potential" [J. Chem. Phys. 118, 8207 (2003)]. *J. Chem. Phys.* **2006**, *124*, No. 219906.

(34) McKenna, K. P.; Shluger, A. L. First-principles calculations of defects near a grain boundary in MgO. *Phys. Rev. B* **2009**, *79*, No. 224116.

(35) Yang, J.-H.; Yin, W.-J.; Park, J.-S.; Metzger, W.; Wei, S.-H. First-principles study of roles of Cu and Cl in polycrystalline CdTe. *J. Appl. Phys.* **2016**, *119*, No. 045104.

(36) Sato, Y.; Mizoguchi, T.; Oba, F.; Yodogawa, M.; Yamamoto, T.; Ikuhara, Y. Atomic and electronic structure of $[0001]/(1230) \sum 7$ symmetric tilt grain boundary in ZnO bicrystal with linear current-voltage characteristic. *J. Mater. Sci.* **2005**, *40*, 3059−3066.

(37) Imaeda, M.; Mizoguchi, T.; Sato, Y.; Lee, H. S.; Findlay, S. D.; Shibata, N.; Yamamoto, T.; Ikuhara, Y. Atomic structure, electronic structure, and defect energetics in $[001](310) \sum 5$ grain boundaries of $SrTiO_3$ and $BaTiO_3$. *Phys. Rev. B* **2008**, *78*, No. 245320.

(38) Wang, Z.; Saito, M.; McKenna, K. P.; Gu, L.; Tsukimoto, S.; Shluger, A. L.; Ikuhara, Y. Atom-resolved imaging of ordered defect superstructures at individual grain boundaries. *Nature* **2011**, *479*, 380.

(39) Kohyama, M. Computational studies of grain boundaries in covalent materials. *Modell. Simul. Mater. Sci. Eng.* **2002**, *10*, R31−R59.

(40) Consonni, V.; Baier, N.; Robach, O.; Cayron, C.; Donatini, F.; Feuillet, G. Local band bending and grain-to-grain interaction induced strain nonuniformity in polycrystalline CdTe films. *Phys. Rev. B* **2014**, *89*, No. 035310.

(41) Flores, M. A.; Orellana, W.; Menéndez-Proupin, E. First-principles DFT+GW study of the Te antisite in CdTe. *Comput. Mater. Sci.* **2016**, *125*, 176−182.